

Accelerating H₂ Evolution by Anodic Semi-dehydrogenation of Tetrahydroisoquinolines in Water over Co₃O₄ Nanoribbon Arrays Decorated Nickel Foam

Ming Xiang,^[a] Zhihua Xu,^{*[a]} Jinghao Wang,^[b] Xiaoqiu Yang,^[a] and Zhaoxiong Yan^{*[a]}

Abstract: Coupling the H₂ evolution reaction in water with thermodynamically favorable organic oxidation reactions is highly desirable, because it can enhance the energy conversion efficiency compared with electrocatalytic water splitting, and produce value-added chemicals instead of O₂ in the anodic reaction. Herein, Co₃O₄ nanoribbon arrays in situ grown on nickel foam (Co₃O₄@NF) was employed as an effective electrocatalyst for the selective oxidation of tetrahydroisoquinolines (THIQs). Various value-added semi-dehydrogenation products including dihydroisoquinolines with electro-deficient or -rich groups could be obtained with moderate yields and faradaic efficiencies. Benefitting from the rich surface active sites of Co₃O₄@NF, a two-electrode (Co₃O₄@NF | Pt) electrolytic system drove a benchmark current density of 10 mAcm⁻² at a cell voltage as low as 1.446 V in 1.0 M KOH aqueous solution containing 0.02 M THIQ, which was reduced by 174 mV in comparison with that of overall water splitting.

Electrocatalytic water splitting is emerging as a promising hydrogen production approach.^[1–4] Due to the sluggish oxygen evolution reaction (OER), a much higher overpotential is needed at anode to match hydrogen evolution reaction (HER) at cathode.^[5–8] In order to tackle this issue, replacing OER with thermodynamically more favorable organic oxidation reaction is considered as an alternative strategy to boost HER.^[9–12] Previously, numerous research efforts focused on organic molecules like urea, hydrazine and various alcohols (including methanol, glycerol and 5-hydroxymethylfurfural) as the more readily oxidized species.^[13–24] Compared with OER, they could not only significantly enhance anodic reaction kinetics, but also

dramatically reduced the working voltage of the whole cell.^[25–26] Nevertheless, oxidizing urea or hydrazine would generate valueless decomposition products (CO₂, H₂O and N₂), and primary alcohol would be usually oxidized into corresponding fully oxidized products (organic acids). Therefore, the development of effective electrocatalyst towards selective transformations of chemicals into semi-oxidized products will be more challenging and worthy.^[27]

Dehydrogenation from N-heterocycles under oxidant-free conditions provided a mild approach to generate unsaturated heteroaromatic compounds with the release of hydrogen gas.^[28–29] However, most reported thermo-, photo- and electrocatalytic synthetic routes should operate in organic solvents, and usually resulted in the complete dehydrogenation products.^[30–34] Recently, Zhang group employed Ni₂P or NiO as the electrocatalyst to achieve the aqueous semi-dehydrogenation of tetrahydroisoquinolines (THIQs) by coupling with effective HER or nitrate reduction reaction, which made a breakthrough in achieving value-added product dihydroisoquinolines (DHIQs).^[27,35] Considering the positive function of DHIQ in pharmaceutical chemistry,^[36–37] it is highly desirable to develop more readily available electrocatalysts especially based on other earth-abundant metal elements, which could integrate the selective oxidation from THIQs to DHIQs with HER in water.

Herein, we report Co₃O₄ nanoribbon arrays in situ decorated nickel foam as highly efficient electrocatalyst (Co₃O₄@NF) for the selective semi-dehydrogenation of THIQs. When adding 0.02 M THIQ into 1.0 M KOH aqueous solution, the voltage requirement for the two-electrode electrolyser (Co₃O₄@NF | Pt) was only 1.446 V to achieve a benchmark current density of 10 mAcm⁻², which not only was reduced by 174 mV in comparison with that of water oxidation, but also accelerated hydrogen production from water reduction. For electron-rich as well as deficient THIQ derivatives, DHIQs could be obtained at Co₃O₄@NF anode with moderate yields and faradaic efficiencies (FEs), which demonstrated potential applications in pharmaceutical synthesis.

The Co₃O₄ nanoribbon arrays were synthesized by a facile hydrothermal process and a subsequent annealing treatment,^[38–39] which were easier to be obtained than the Ni₂P electrode from the aspect of experimental operation. X-ray diffraction (XRD) was employed to confirm the crystalline phase of the Co₃O₄ deposit. As shown in Figure 1a, both the synthesized sample and the bare NF sample showed three characteristic peaks at 45.1, 52.4 and 77.0° attributed to the diffraction peaks of the pristine Ni foam (PDF 04–0850). Due to the strong signal of the substrate NF, the weak diffraction peaks

[a] Dr. M. Xiang, Prof. Dr. Z. Xu, X. Yang, Dr. Z. Yan
Key Laboratory of Optoelectronic Chemical Materials and Devices of
Ministry of Education
Jiangnan University, Wuhan 430056 (P. R. China)
E-mail: xuzhihua78@sina.com
zhaoxiongyan75@163.com

[b] Dr. J. Wang
CAS Key Laboratory of Nanosystem and Hierarchical Fabrication
CAS Center for Excellence in Nanoscience
National Center for Nanoscience and Technology, Beijing 100190 (P. R.
China)

Supporting information for this article is available on the WWW under
<https://doi.org/10.1002/chem.202100249>

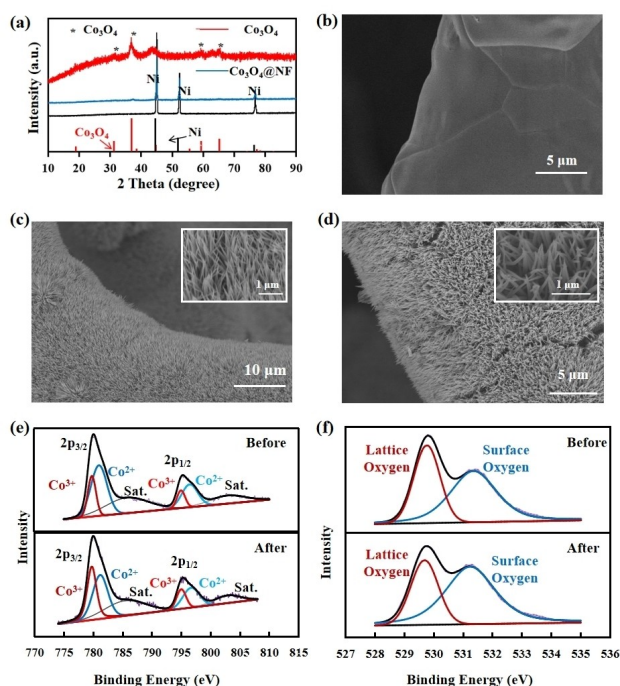


Figure 1. (a) XRD patterns of NF, Co_3O_4 @NF and exfoliated Co_3O_4 . SEM images for bare NF (b), Co_3O_4 @NF before (c) and after (d) electrocatalytic THIQ oxidation. XPS spectra in the Co 2p region (e) and the O 1s region (f) for Co_3O_4 before (top) and after (bottom) electrocatalytic THIQ oxidation.

of the Co_3O_4 deposit were masked. After peeling off the black deposit from the NF, the power XRD pattern revealed a set of broad peaks marked with asterisks at 31.6 , 36.9 , 59.5 and 65.4° , which precisely coincided with the (220), (311), (511) and (440) planes of the cubic phase of Co_3O_4 (PDF 43–1003), respectively. The morphology of Co_3O_4 nanoribbon arrays grown on the surface of Ni foam was measured by the scanning electron microscopy (SEM). Compared with the smooth surface of the bare Ni foam (Figure 1b), the Co_3O_4 @NF sample displays a vertically uniform coating of Co_3O_4 nanoribbon arrays (Figure 1c). The rough surface morphology supplied a high specific surface area, which can deliver sufficient contact area for the reaction substrates. X-ray photoelectron spectroscopy (XPS) was carried out to identify the element compositions of the synthesized sample. Two distinct peaks with binding energies at 779.9 and 795.1 eV (Figure 1e top) were attributed to Co 2p_{3/2} and Co 2p_{1/2} spin-orbit peaks of the Co_3O_4 phase, respectively. Meanwhile, the O 1s XPS spectra peak at a binding energy value of around 529.8 eV was assigned to oxygen species in the Co_3O_4 phase (Figure 1f top).^[40–41] All the above results clearly confirmed the successful modification of Co_3O_4 nanoribbon arrays on nickel foam.

In order to evaluate the electrocatalytic performance of the Co_3O_4 @NF electrode for the anodic semi-dehydrogenation transformation, 1,2,3,4-tetrahydroisoquinoline **1a** was selected as a model substrate. All the electrochemical measurements were carried out in a standard three-electrode system. The anodic reaction was first investigated by applying the linear sweep voltammetry (LSV) method with or

without the presence of **1a** (Figure 2a). For the Co_3O_4 @NF electrode, a steep curve appeared at about 1.50 V versus RHE (reversible hydrogen electrode) in the absence of **1a**, with the appearance of O_2 bubbles at the surface of anode. Besides, two oxidation peaks at about 1.25 V and 1.45 V could be attributed to $\text{Co}^{\text{II}}/\text{Co}^{\text{III}}$ and $\text{Co}^{\text{III}}/\text{Co}^{\text{IV}}$, respectively.^[42–43] After adding 0.02 M **1a** in 1.0 M KOH, the current density increased dramatically at about 1.30 V, mainly contributed by the oxidation current of THIQ. It implied that THIQ oxidation was thermodynamically more favorable than water oxidation over the Co_3O_4 modified electrode. As for the NF electrode, the enhancement of anodic current was very small after adding **1a**. Thus, we speculated that the oxidation of **1a** primarily depended on the Co_3O_4 electrocatalyst, not the NF substrate, which was different from the previous reports.^[33,34] Thus, it could be deduced that Co_3O_4 could also effectively catalyze dehydrogenation of N-heterocycles, and the Ni foam here was mainly functioned as the substrate providing a high specific surface area to immobilize the Co_3O_4 nanoribbon arrays. Subsequently, we examined the effect of potential on the semi-dehydrogenation reaction. A series of long-term chronoamperometry at different potentials from 1.25 to 1.60 V were carried out with 0.02 M **1a** (Figure 2b). At 1.25 V, target product **2a** was generated with FE of about 98% and selectivity of nearly 100%. However, the electrocatalytic reaction was too slow at this potential, resulting in retention of most substrate **1a**. At the potentials from 1.30 to 1.60 V, after passing a theoretical charge of 38.5 C for the semi-dehydrogenation of **1a** to **2a**, the products were collected. Both FEs and selectivities for this transformation decreased with increasing anodic potential. At 1.30 and 1.35 V, the optimal results were obtained with FEs of about 75% and selectivities of about 90%. Furthermore, the substrate **1a** remained and the product **2a** generated at different reaction times were collected at the constant potential of 1.35 V (Figure 2c). A charge of 37 C would be passed within 1 hour,

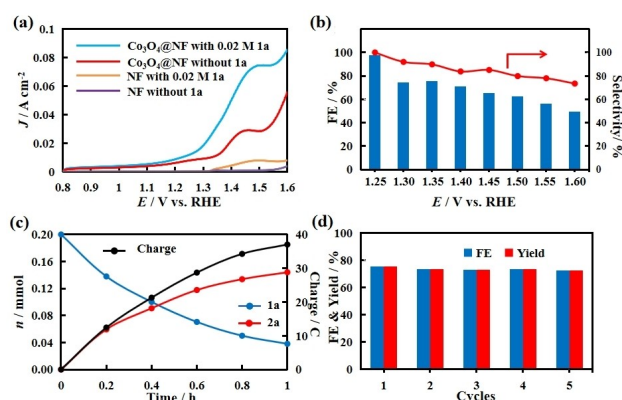


Figure 2. (a) LSV curves of the Co_3O_4 @NF or NF anode at a scan rate of 10 mV s^{-1} in 10 mL of 1.0 M KOH with or without 0.02 M **1a**. (b) FEs and selectivities of **2a** production at different potentials. (c) Conversion of **1a** and yield of its semi-dehydrogenation product **2a** over passed charge. (d) FEs and yields of **2a** production after passing a charge of 38.5 C under five successive cycles. Chronoamperometry experiments of (b), (c) and (d) were conducted in 10 mL of 1.0 M KOH containing 0.02 M **1a**.

and the retaining **1a** was 19% with 72% yield of **2a**. It indicated that most **1a** could be transformed into **2a** quickly at 1.35 V. The durability test for the $\text{Co}_3\text{O}_4/\text{NF}$ anode was also investigated. After five consecutive runs of chronoamperometry experiment at 1.35 V, no remarkable loss of the activity was observed based on the DHIQ yields (Figure 2d). SEM image of the $\text{Co}_3\text{O}_4/\text{NF}$ electrode after stability test (Figure 1d) showed that the nanoribbon array morphology was still maintained on the surface of NF substrate without obvious peeling off from the NF, anticipating its robust electrochemical stability for this electrocatalytic semi-dehydrogenation.

To further gain insight into the catalytic activity of $\text{Co}_3\text{O}_4/\text{NF}$ electrode for the semi-dehydrogenation of THIQ, more electrochemical parameters were measured. As shown in Figure 3a, the cyclic voltammograms (CVs) over $\text{Co}_3\text{O}_4/\text{NF}$ electrode were performed. An enhanced anodic current and an obvious decreased cathodic current between 1.30 and 1.65 V were observed in the presence of **1a** compared with those in the absence of **1a**. The enhanced anodic current was due to the oxidation of **1a** by the electrochemically generated higher-valence cobalt species, as well as the direct electro-oxidation of **1a** on the electrode. Since part of higher-valence cobalt species was reduced by **1a**, the reduction current of higher-valence cobalt species decreased. The above phenomenon was an indication that the cobalt catalyst of variable valence, as a redox mediator like TEMPO³², was involved in the reaction to promote the anodic oxidation of **1a**. Not only that, the ratio of $\text{Co}^{3+}/\text{Co}^{2+}$ increased after semi-dehydrogenation reaction by a careful comparison of the area change of Co^{3+} and Co^{2+} in the high-resolution XPS spectra (Figure 1e and Table S1). Therefore, we speculated that Co^{2+} could be converted to Co^{3+} , and Co^{3+} then captured an electron from **1a** to go back to Co^{2+} during the electrocatalytic oxidation process. Tafel tests were carried out to investigate the kinetic processes of the oxidation reaction over the electrocatalysts (Figure 3b). The $\text{Co}_3\text{O}_4/\text{NF}$ electrode

showed a tafel slope of 137 mVdec^{-1} for oxygen evolution reaction. Meanwhile, it is noted that a competitive tafel slope of 129 mVdec^{-1} for the oxidation of **1a** was observed at a much lower potential region, indicating that the Co_3O_4 modified NF exhibited a superior oxidation activity for **1a**. Considering that the double-layer capacitance could reflect the electrochemically active surface area, we determined cyclic voltammograms recorded in the non-faradaic potential range to calculate the double-layer capacitance (Figure S4). After loading Co_3O_4 on nickel foam, the double-layer capacitance improved from 3.2 mF cm^{-2} to 245.6 mF cm^{-2} , suggesting that the Co_3O_4 nanoribbon arrays offered a much higher number of electrocatalytically active sites for THIQ electrooxidation (Figure 3c). Besides, the fitted O 1s XPS peak at about 531.4 eV was assigned to the surface oxygen species (eg. hydroxyls) of the electrocatalyst (Figure 1f top). The abundance of absorbed oxygen species on the anode surface could capture THIQ via hydrogen bonding, and favor its subsequent electrooxidation. So it was reasonable to speculate that the surface oxygen species could modulate the surface state of catalytically active sites and improve the oxidative ability of Co_3O_4 modified anode. It was found that the proportion of surface oxygen species increased after electrocatalytic oxidation (Figure 1f and Table S2), which might contribute to the stability of the $\text{Co}_3\text{O}_4/\text{NF}$ anode. The electrochemical impedance spectroscopy (EIS) measurements were employed to further evaluate the effect of Co_3O_4 modification. A non-ideal semicircle was observed when using the pristine nickel foam as anode, however, the semicircle nearly disappeared in the case of $\text{Co}_3\text{O}_4/\text{NF}$ electrode (Figure 3d and Table S3). It revealed that the THIQ oxidation was limited by the mass transport due to the fast electron transfer between Co_3O_4 catalyst and THIQ.

Furthermore, some representative tetrahydroisoquinoline derivatives were examined to explore the generality of this electrocatalytic oxidation method over the $\text{Co}_3\text{O}_4/\text{NF}$ electrode. As summarized in Figure 4a, various THIQs containing electron-deficient or rich groups on the aromatic ring were smoothly converted to the corresponding semi-dehydrogenation products in moderate yields (**2b–2e**, 64%–70%). Notably, our reaction system could operate in an undivided cell and in air atmosphere at room temperature, which was convenient and avoided preparing specific electrochemical cell. We assembled a two-electrode electrolyzer with $\text{Co}_3\text{O}_4/\text{NF}$ as an anode and platinum plate as a cathode. Compared with overall water splitting, the $\text{Co}_3\text{O}_4/\text{NF}||\text{Pt}$ exhibited much better energy conversion efficiency after adding 0.02 M **1a** (Figure 4b). For instance, the required voltage for achieving the current density of 10 mA cm^{-2} shifted from 1.620 V (without **1a**) to 1.446 V (with **1a**), confirming again that oxidation of THIQ was thermodynamically more favorable than OER (inset of Figure 4b). Besides, such a two-electrode configuration was applied to couple semi-dehydrogenation of **1a** and HER with an applied voltage in the range of 1.5 to 1.7 V (Figure 4c). No apparent decrease of FEs and selectivities were observed below the

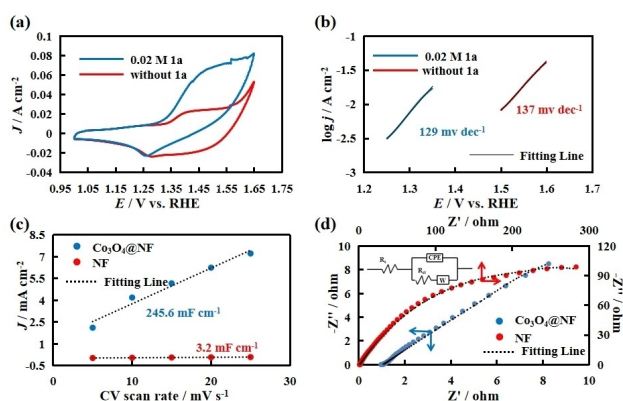


Figure 3. (a) CV curves of a $\text{Co}_3\text{O}_4/\text{NF}$ anode at a scan rate of 10 mV s^{-1} and (b) Tafel plots of a $\text{Co}_3\text{O}_4/\text{NF}$ anode based on LSV curves at a scan rate of 2 mV s^{-1} in 1 M KOH with or without 0.02 M **1a**. (c) The capacitive current density at 1.15 V as a function of CV scan rate and (d) Nyquist plots in the frequency range from 0.01 Hz to 100 kHz in 1 M KOH with 0.02 M **1a** (inset: the equivalent circuit).

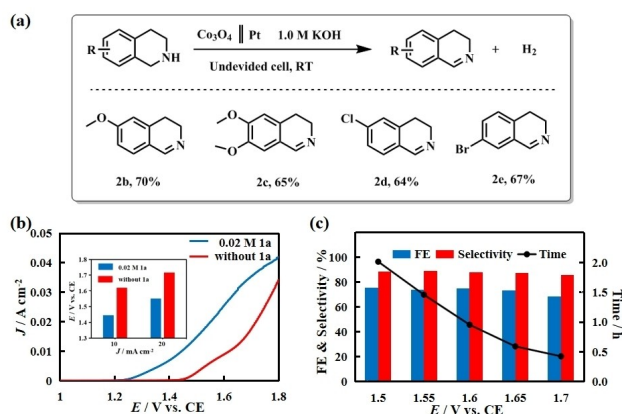


Figure 4. (a) Reaction conditions: THIQs (0.2 mmol), Co_3O_4 @NF anode (working area: 0.9 cm^2), Pt cathode, 1.0 M KOH (10 mL), room temperature, 0.35 V vs. Ag/AgCl, passing charge of 38.5 C. Isolated Yields. (b) LSV curves and cell voltage comparison for achieving benchmark current densities (10 and 20 mA cm^{-2}) over a Co_3O_4 @NF | Pt electrolyzer in 1.0 M KOH with or without 0.02 M **1a**. (c) FEs and selectivities of a Co_3O_4 @NF | Pt electrolyzer for **2a** production at different cell voltages in 1.0 M KOH solution with 0.02 M **1a**.

cell voltage of 1.65 V, which offered a relatively broad operation window for possible industrial application.

In summary, we have successfully accelerated electrocatalytic H_2 production in water through substituting the OER with the selective semi-dehydrogenation of THIQs over the Co_3O_4 @NF anode. In situ anchoring of Co_3O_4 nanoarrays on the surface of nickel foam not only provided densely electrocatalytic active sites for THIQ oxidation with much fast kinetics, but also achieved conversion of various THIQs into DHIQs with moderate yields, selectivities and good substrate compatibilities. Impressively, the Co_3O_4 @NF anode can be integrated with platinum plate cathode for semi-dehydrogenation of THIQs and energy-saving HER respectively, in a two-electrode electrolyzer. Compared with the overall water splitting, the cell voltage was dramatically reduced from 1.620 V to 1.446 V at the current density of 10 mA cm^{-2} with THIQ participation. On account of the facile preparation and robust durability of the Co_3O_4 @NF electrode, this work may open an economical and highly efficient route to produce both hydrogen and value-added DHIQs.

Acknowledgements

This work was financially supported by the National Natural Science Foundation of China (No. 21871111), Excellent Youth Foundation of Hubei Province of China (No. 2019CFA078) and the Opening Project of Key Laboratory of Optoelectronic Chemical Materials and Devices, Ministry of Education, Jiangnan University (No. JDGD-202012).

Conflict of Interest

The authors declare no conflict of interest.

Keywords: Co_3O_4 electrocatalyst · dihydroisoquinolines · energy-saving · hydrogen evolution reaction · semi-dehydrogenation

- [1] J. Hou, Y. Wu, B. Zhang, S. Cao, Z. Li, L. Sun, *Adv. Funct. Mater.* **2019**, *29*, 1808367.
- [2] J. Wang, W. Cui, Q. Liu, Z. Xing, A. M. Asiri, X. Sun, *Adv. Mater.* **2016**, *28*, 215–230.
- [3] Y. Yu, Y. Shi, B. Zhang, *Acc. Chem. Res.* **2018**, *51*, 1711–1721.
- [4] J. Zhang, Q. Zhang, X. Feng, *Adv. Mater.* **2019**, *31*, 1808167.
- [5] C. C. L. McCrory, S. Jung, I. M. Ferrer, S. M. Chatman, J. C. Peters, T. F. Jaramillo, *J. Am. Chem. Soc.* **2015**, *137*, 4347–4357.
- [6] T. Reier, H. N. Nong, D. Teschner, R. Schloegl, P. Strasser, *Adv. Energy Mater.* **2017**, *7*, 1601275.
- [7] Q. Shi, C. Zhu, D. Du, Y. Lin, *Chem. Soc. Rev.* **2019**, *48*, 3181–3192.
- [8] K. Zeng, D. Zhang, *Prog. Energy Combust. Sci.* **2010**, *36*, 307–326.
- [9] Y. X. Chen, A. Lavacchi, H. A. Miller, M. Bevilacqua, J. Filippi, M. Innocenti, A. Marchionni, W. Oberhauser, L. Wang, F. Vizza, *Nat. Commun.* **2014**, *5*, 4036.
- [10] Y. Xu, B. Zhang, *ChemElectroChem* **2019**, *6*, 3214–3226.
- [11] B. You, X. Liu, N. Jiang, Y. Sun, *J. Am. Chem. Soc.* **2016**, *138*, 13639–13646.
- [12] B. You, Y. Sun, *Acc. Chem. Res.* **2018**, *51*, 1571–1580.
- [13] X. Deng, M. Li, Y. Fan, L. Wang, X.-Z. Fu, J.-L. Luo, *Appl. Catal. B* **2020**, *278*, 119339.
- [14] L. Gao, J. Xie, S. Liu, S. Lou, Z. Wei, X. Zhu, B. Tang, *ACS Appl. Mater. Interfaces* **2020**, *12*, 24701–24709.
- [15] Z. Ji, J. Liu, Y. Deng, S. Zhang, Z. Zhang, P. Du, Y. Zhao, X. Lu, *J. Mater. Chem. A* **2020**, *8*, 14680–14689.
- [16] H. J. Kim, Y. Kim, D. Lee, J.-R. Kim, H.-J. Chae, S.-Y. Jeong, B.-S. Kim, J. Lee, G. W. Huber, J. Byun, S. Kim, J. Han, *ACS Sustainable Chem. Eng.* **2017**, *5*, 6626–6634.
- [17] W.-J. Liu, L. Dang, Z. Xu, H.-Q. Yu, S. Jin, G. W. Huber, *ACS Catal.* **2018**, *8*, 5533–5541.
- [18] C. Tang, R. Zhang, W. Lu, Z. Wang, D. Liu, S. Hao, G. Du, A. M. Asiri, X. Sun, *Angew. Chem. Int. Ed.* **2017**, *56*, 842–846; *Angew. Chem.* **2017**, *129*, 860–846.
- [19] Y. Tong, P. Chen, M. Zhang, T. Zhou, L. Zhang, W. Chu, C. Wu, Y. Xie, *ACS Catal.* **2018**, *8*, 1–7.
- [20] G. Yang, Y. Jiao, H. Yan, Y. Xie, A. Wu, X. Dong, D. Guo, C. Tian, H. Fu, *Adv. Mater.* **2020**, *32*, 2000455.
- [21] B. You, N. Jiang, X. Liu, Y. Sun, *Angew. Chem. Int. Ed.* **2016**, *55*, 9913–9917; *Angew. Chem.* **2016**, *128*, 10067–9917.
- [22] Z.-Y. Yu, C.-C. Lang, M.-R. Gao, Y. Chen, Q.-Q. Fu, Y. Duan, S.-H. Yu, *Energy Environ. Sci.* **2018**, *11*, 1890–1897.
- [23] J.-Y. Zhang, H. Wang, Y. Tian, Y. Yan, Q. Xue, T. He, H. Liu, C. Wang, Y. Chen, B. Y. Xia, *Angew. Chem. Int. Ed.* **2018**, *57*, 7649–7653; *Angew. Chem.* **2018**, *130*, 7775–7653.
- [24] B. Zhao, J.-W. Liu, Y.-R. Yin, D. Wu, J.-L. Luo, X.-Z. Fu, *J. Mater. Chem. A* **2019**, *7*, 25878–25886.
- [25] G. Dodekatos, S. Schuenemann, H. Tueysuez, *ACS Catal.* **2018**, *8*, 6301–6333.
- [26] B. You, G. Han, Y. Sun, *Chem. Commun.* **2018**, *54*, 5943–5955.
- [27] C. Huang, Y. Huang, C. Liu, Y. Yu, B. Zhang, *Angew. Chem. Int. Ed.* **2019**, *58*, 12014–12017; *Angew. Chem.* **2019**, *131*, 12142–12017.
- [28] N. O. Balayeva, Z. Mamiyev, R. Dillert, N. Zheng, D. W. Bahnemann, *ACS Catal.* **2020**, *10*, 5542–5553.
- [29] Q. Yin, M. Oestreich, *Angew. Chem. Int. Ed.* **2017**, *56*, 7716–7718; *Angew. Chem.* **2017**, *129*, 7824–7718.
- [30] S. Chakraborty, W. W. Brennessel, W. D. Jones, *J. Am. Chem. Soc.* **2014**, *136*, 8564–8567.
- [31] S. Kato, Y. Saga, M. Kojima, H. Fuse, S. Matsunaga, A. Fukatsu, M. Kondo, S. Masaoka, M. Kanai, *J. Am. Chem. Soc.* **2017**, *139*, 2204–2207.
- [32] Y. Wu, H. Yi, A. Lei, *ACS Catal.* **2018**, *8*, 1192–1196.
- [33] A. Reyes-Sánchez, F. Cañavera-Buelvas, R. Barrios-Francisco, O. L. Cifuentes-Vaca, M. Flores-Alamo, J. J. García, *Organometallics* **2011**, *30*, 3340–3345.
- [34] S. Bera, A. Bera, D. Banerjee, *Org. Lett.* **2020**, *22*, 6458–6463.
- [35] Y. Wang, C. Liu, B. Zhang, Y. Yu, *Sci. China Mater.* **2020**, *63*, 2530–2538.
- [36] O. V. Surikova, A. S. Yusov, R. R. Makhmudov, A. G. Mikhailovskii, *Pharm. Chem. J.* **2017**, *51*, 18–21.

- [37] J. Ziemska, A. Guspiel, J. Jarosz, A. Nasulewicz-Goldeman, J. Wietrzyk, R. Kawecki, K. Pypowski, M. Jaroriczek, J. Solecka, *Bioorg. Med. Chem.* **2016**, *24*, 5302–5314.
- [38] Z. Zhou, C. Chen, M. Gao, B. Xia, J. Zhang, *Green Chem.* **2019**, *21*, 6699–6706.
- [39] G. Huang, P. Lou, G.-H. Xu, X. Zhang, J. Liang, H. Liu, C. Liu, S. Tang, Y.-C. Cao, S. Cheng, *J. Alloys Compd.* **2020**, *817*, 152753.
- [40] B. Varghese, C. H. Teo, Y. Zhu, M. V. Reddy, B. V. R. Chowdari, A. T. S. Wee, V. B. C. Tan, C. T. Lim, C.-H. Sow, *Adv. Funct. Mater.* **2007**, *17*, 1932–1939.
- [41] Z.-S. Wu, W. Ren, L. Wen, L. Gao, J. Zhao, Z. Chen, G. Zhou, F. Li, H.-M. Cheng, *ACS Nano* **2010**, *4*, 3187–3194.
- [42] T. Zhou, P. Lu, Z. Zhang, Q. Wang, A. Umar, *Sens. Actuat. B Chem.* **2016**, *235*, 457–465.
- [43] G. Dai, J. Xie, C. Li, S. Liu, *J. Alloys Compd.* **2017**, *727*, 43–51.

Manuscript received: January 21, 2021
Accepted manuscript online: March 26, 2021
Version of record online: April 14, 2021